Physica Scripta. Vol. 66, 133–139, 2002

Krypton Spectrum in the Wavelength Range 3450–3900 Å

H. Chen[1], P. Beiersdorfer[1], C. L. Harris[2] and S. B. Utter[1]

[1] Department of Physics, Lawrence Livermore National Laboratory, Livermore, CA 94551, USA,
[2] Department of Physics, University of Nevada Reno, Reno, NV 89557, USA

Received February 7, 2001; revised version received February 3, 2002; accepted February 11, 2002

PACS Ref: 32.30.Jc, 39.30.+w, 07.60.-j

Abstract

Using a high-efficiency, high-resolution transmission grating spectrometer, we measured krypton spectra over the wavelength range 3450–3900 Å in the low-energy electron beam ion trap EBIT-II at Lawrence Livermore National Laboratory. In total, we analyzed 78 line features, of which only about 20 lines are listed in standard databases. Their wavelengths were determined with accuracy of 0.2–0.5 Å. Different widths of lines from near-neutral and highly-ionized krypton atoms are attributed to ion motion and to the radial extent of the trapped-ion cloud.

1. Introduction

Optical spectral data of krypton are of particular interest for the diagnostics of laboratory fusion plasmas. As a potential radiation medium, Kr can be used to establish a radiative cooling cushion in the edge and divertor regions of large-tokamak and stellarator fusion plasmas [1,2]. Information from the observation of Kr spectral lines can be used to determine local plasma conditions such as fluctuations, radiation and transport, which are fundamentally important to understanding the performance of radiative divertor and the effects of impurity injection as well as the confinement of the fusion plasma.

Previous measurements of the optical spectrum of Kr mostly concerned low-charge state Kr (Kr I to Kr III) spectral lines that were observed using low-pressure vapor lamps (Geissler tubes) in the 1930s [3–6], and a number of wavelengths were then determined with very high precision. In recent years, several measurements have also been made on electric-dipole forbidden transitions of highly charged Kr ions [7–11]. However, as is shown in this paper, the optical regime contains many more lines than tabulated in the earlier work. Most of these optical Kr lines have never been identified.

Our optical measurements used the low-energy electron beam ($E \leqslant 35$ keV) ion trap EBIT-II at Lawrence Livermore National Laboratory [12]. EBIT-II provides ions with charge states appropriate to fusion plasmas, at particle densities that also are comparable to those in laboratory fusion plasmas [13]. Moreover, EBIT-II provides a well-confined ion plasma that permits steady-state measurements of ion spectra. In this paper, we present the results of measurements on krypton that employed a novel transmission grating spectrometer with a nominal maximum spectral resolving power exceeding 15 000. This instrument was previously optimized for work on the Livermore electron beam ion traps [14,15] to detect the faint emission of the 1s hyperfine transitions of hydrogen-like heavy ions.

2. Experimental set-up and data analysis

Kr was injected into our electron beam ion trap using a differentially pumped gas injector. The gas plume intersects the electron beam at right angles. The quantity of the injection was controlled so that the ion density in the trap was on the order of 10^8–10^9 cm^{-3}. Along the drift tube axis (and magnetic field direction), the ions were confined by an electric potential difference applied between the middle and the outer drift tubes. The trapped ion cloud was periodically dumped (by lowering one of the outer drift tube voltages) in order to avoid the accumulation of ions from heavier elements such as tungsten that are emitted in low quantities by the electron gun filament.

The optical Kr spectrum was dispersed using a transmission grating spectrometer LTGS-I [14,15]. The spectrometer uses a high-efficiency grating of 15 cm diameter, with a transmission efficiency of approximately 94% at 3510 Å [16]. The two lenses needed to first provide parallel light for the grating and then focus the diffracted light onto the detector had an aperture ratio of f/4.6. As measured with a standard platinum lamp and a 30 μm wide spectrometer slit, the resolving power of the spectrometer system can be as high as about 15 500 at 3875 Å. In our observations on EBIT-II, the resolving power of the instrument was somewhat lower, because we did not use any physical entrance slit, but exploited the small lateral extent of the light source directly, in order to make optimum use of the available light emission. For short-lived levels excited by the electron beam, this implies a width of the light-emitting zone that is close to that of the electron beam itself. This typical width of 60 μm is a factor of 2 wider than the slit used in the offline testing of the spectrometer. Moreover, spectral lines emitted by ions in EBIT-II are broadened by the thermal ion motion (Doppler broadening). Further line broadening occurs when lines from metastable ions are observed, because ions excited to long-lived levels may leave the excitation volume before they emit radiation, and the actual trapped-ion cloud may extend well outside the electron beam. The full-width at half-maximum (FWHM) of a typical spectral line from low-charge state ions in our spectra is 0.92 Å (see Fig. 1), corresponding to an effective spectral resolving power of about 3800. By contrast, the observed width of lines from highly charged trapped Kr ions is about 1.5 Å (see Fig. 2), which corresponds to an effective spectral resolution of 2600. If we assumed that the increased broadening was due solely to the ion motion, we could infer an ion temperature of about 1100 eV. This temperature agrees with values measured under similar experimental conditions using high-resolution crystal spectrometers [17,18]. If we assumed that the line width instead was the result of source broadening, we would infer an "effective" ion cloud radius which is about 1.6 times that of the electron beam. Such broadening was

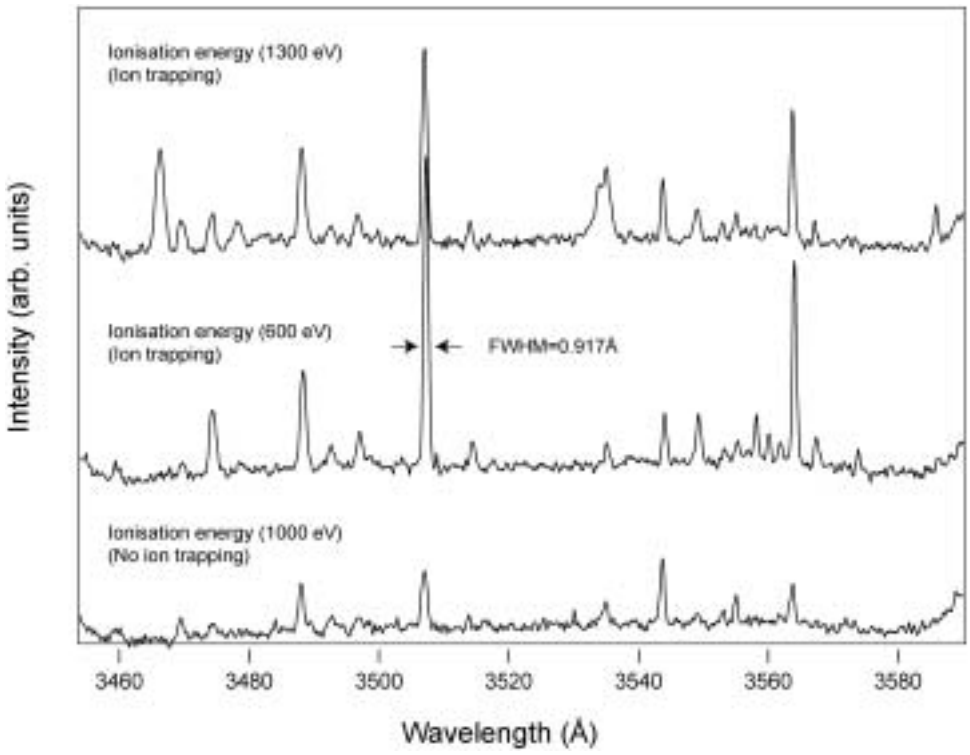

Fig. 1. Sections of Kr spectra at three electron beam energies: 1300 eV (top), 600 eV (middle) and 1000 eV (bottom). The upper two spectra were taken in the electron trapping mode, while the bottom spectrum was observed in the inverted trapping mode.

inferred from other measurements of metastable optical lines [11]. Similar observations, but from direct imaging of the ion cloud onto a CCD camera, have recently been reported from the NIST EBIT [19]. Of course, we expect that both Doppler broadening and source broadening contribute to the overall line width observed.

A cryogenically cooled CCD camera was employed to record the spectrum. The CCD chip had 1024×1024 pixels of size $24\,\mu m \times 24\,\mu m$, and each CCD image covered a wavelength range of about 120 Å. In order to cover the wavelength range from 3450 Å to 3900 Å, the CCD camera was set to four different positions located along the focal plane of the imaging lens of the spectrometer. We allowed ample spectral overlap between adjacent camera positions. To enhance the signal-to-noise ratio and to reduce the signal read-out time, CCD pixels were binned in groups of four in the non-dispersion direction. Each krypton spectrum was taken with a 20-minute exposure. Right after each Kr spectrum, a 20-minute-exposure background spectrum was taken with the gas injection switched off. This allowed us to subtract from the raw Kr spectra most of the background emission that among other contributions originates from intrinsic impurities.

3. Data analysis

Each spectral line was fitted with a Gaussian function to its line profile. The wavelength calibration of the spectrometer system used well-known lines from singly and doubly ionized Ne, Ar and Kr atoms and was accomplished in situ. Calibration spectra were obtained with EBIT running in inverted-trap mode [14,20]. The inverted-trap mode is arranged by removing the electric potentials applied to the end electrodes of the trap, so that any ions in the trap region are actively expelled from the trap volume. Injected atoms (from the ballistic gas injector) cross through the electron beam; the interaction time between atoms in the gas plume and the electron beam is sufficient for atoms to be ionized singly, or at most a very few times. Spontaneous decays of the typical nanosecond-lifetime excited levels take place in or very near to the electron beam volume.

The wavelengths of many optical lines from singly to triply ionized Ne, Ar, and Kr atoms have been previously measured with high precision, and the data are well documented in existing databases [21,22]. The lines used for the calibration of our spectra are listed in Table I. To obtain the spectrometer dispersion function, the calibration lines were fitted to a linear function using the Least Chi-square fit for each measurement position. Although the focal plate of the grating is not perfectly flat across whole measurement positions, linear fits give very good approximations in all cases; the Linear Correlation Coefficients are from 0.99998 to 1. The resulting dispersion of the spectrometer is 0.1390 ± 0.0004 Å/channel.

Small spectral shifts (up to 5 CCD pixels) were observed during the course of our measurements, which we attribute to changes in the surrounding conditions such as mechanical vibrations and temperature variations. These shift were actively tracked by using some strong lines served for in situ calibrations. This way, we were able to reduce uncertainties of the line wavelengths caused by this shift. However, the shift has not been systematically measured and total correction was not possible. This shift increases the wavelength uncertainties over those expected from the resolving power of the spectrometer.

We determined the uncertainty on the measured wavelengths by analyzing the statistical fitting error of each line as well as the uncertainty from the calibration which

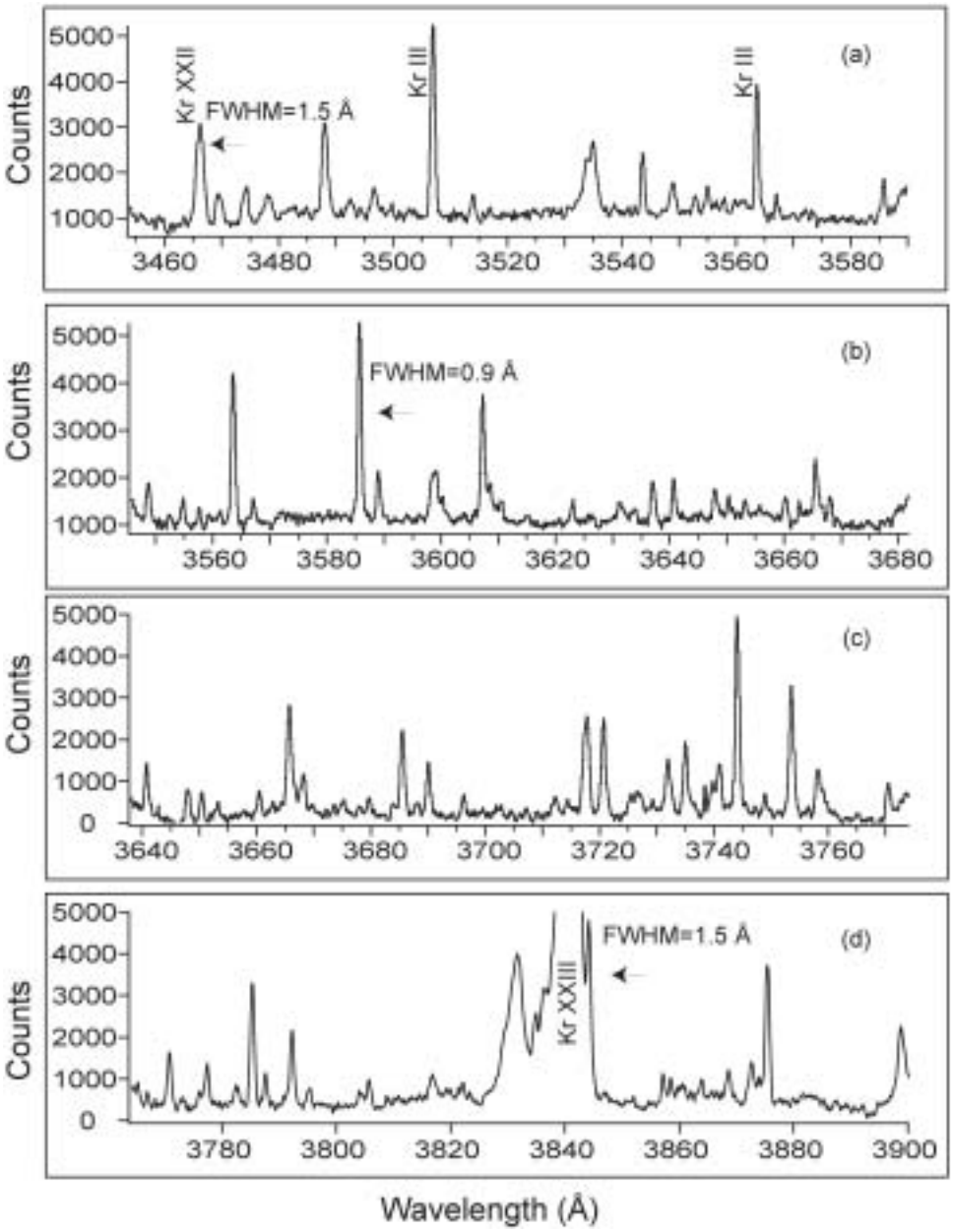

Fig. 2. Kr spectra recorded at an electron beam energy of 1300 eV at four camera positions in the focal plane of the transmission grating spectrometer. The width of several lines is indicated to illustrate the observed range. The wavelengths of all spectral features and their relative intensities are listed in Table III.

Table I. *Lines used for the in situ calibration in the present measurements.*

Ion	Wavelength (Å)	Ion	Wavelength (Å)
Ne II	3459.32	Kr III	3564.23
Ne II	3479.52	Ne II	3568.5
Ne II	3480.72	Ne II	3574.18
Kr III	3488.59	Ne II	3574.61
Ar III	3499.67	Ar II	3582.355
Ar III	3503.58	Ar I	3606.522
Kr III	3507.42	Kr II	3607.88
Ar II	3509.778	Ar II	3639.833
Ar III	3511.12	Ne II	3643.93
Ar II	3514.388	Ne II	3664.07
Ne I	3520.472	Kr III	3690.65
Ne II	3542.85	Kr II	3754.245
Ar II	3545.596	Kr II	3778.089
Ar II	3545.846	Kr II	3783.095
Ar II	3559.508	Kr III	3868.70
Ar II	3561.03	Kr II	3875.44

was estimated as the maximum possible residual from the calibration fitting. The total uncertainty given for the inferred wavelengths then are the summation of the two.

The relative intensity of each line was determined by normalizing to the strongest line: Si-like Kr^{22+}, which is of a magnetic dipole (M1) transition ($3s^2 3p^2\,{}^3P_1$-$^3P_2$). The intensity of this line was defined as 1000. To present the relative intensity across the whole coverage of the measurement, we used the spectra measured at the same electron beam energy (1300 eV) at all camera positions, keeping the experimental conditions as constant as possible. Further adjustments were made for spectra from different positions by normalizing the intensities of lines in the overlap regions of adjacent measurement positions. The detection efficiency was assumed to be constant across the spectral region. Due to the steep rising of the CCD baseline (mostly from readout noise and thermal noise) at both ends of the CCD chip (the first and last ~50

channels, equivalent to about 7 Å for each CCD image), this baseline could not be completely subtracted from the Kr spectra (see Figs 1 and 2). During our relative intensity analysis, we discard data from these end regions because there is have sufficient spectral overlap among spectra taken at different detector positions.

4. Results and discussion

Kr spectra were taken at selected specific electron beam energies. The beam energies were chosen so that each increment corresponds to an increase of the highest ionization stage reached by one unit of charge. However, limited by the minimum electron beam energy at which the electron beam is stable and sufficient signal rate can be obtained, which was about 150 to 200 eV, we cannot distinguish by charge state the lines of neutral and a few times ionized Kr ions. One possible way of narrowing down this number of charge states is using the "inverted trap" technique as mentioned above. Since most of the spectral lines that show in the spectra from an inverted trap are produced by ions with a charge lower than 3 or 4, we can distinguish ions in the first few ionization stages from all those ions of higher charge states. Above the minimum beam energy, desired maximum-charge states were successfully selected by varying the beam energy.

In total, we recorded Kr spectra over a range of twenty electron beam energies from 200 eV to 5000 eV. Our measurements scanned through Kr charge states from neutral Kr to He-like Kr. A typical set of spectra from our measurements is shown in Fig. 2. While most of the charge state distribution encompasses just a few charge states near the maximum possible (given by the largest ionization potential not exceeding by the electron beam energy), lines from neutral Kr and low charge-states (Kr I to Kr V) were nevertheless also present in the spectra recorded at high electron beam energies, because neutral Kr gas was fed continually into the trap.

Although most of the resonance lines of highly charged ions are in the X-ray region, some forbidden lines of these ions appear in the optical region. Several optical lines have been observed from highly charged Kr (Kr X to Kr XXVIII). They are summarized in Table II. The strongest line observed is at 3841.1 Å. It appears in spectra recorded at an electron energy of 970 eV and higher, which is just above the ionization energy of Kr XXIII. This line has been identified with the well-known magnetic dipole (M1) transition of Si-like Kr^{22+} ($3s^2 3p^2\,{}^3P_1$-$^3P_2$), and it has been observed in a tokamak fusion plasma at 3840.9 ± 0.3 Å [7] as well as in various electron beam ion trap devices [8–10]; theory predicts this line at 3832 Å [23]. The line has been measured before on EBIT-II with LTGS-I, and its wavelength had been determined to be 3841.4 ± 0.2 Å [11]. In the present measurement we determine its wavelength to be 3841.1 ± 0.2 Å. The present wavelength value is slightly lower than the previous measurement, but this within the combined 1σ error bars. Moreover, the line was found to have peculiar features [11], as illustrated in Fig. 2, which shows details of the base of the line; these complicate the determination of the centroid of the line. Also, we cannot rule out blending with weaker lines from low charge state ions, as has been noted in [11], although the line is so strong that such blends should have a negligible effect.

The second strongest line in our spectra is at 3466.6 ± 0.2 Å. This line appeared in spectra recorded at an electron energy of 900 eV and higher, and it is therefore identified with Kr XXII. This line has previously been measured at 3464.7 ± 0.6 Å at the NIST EBIT [8] and has been identified with the M1 transition Kr XXII $3s^2 3p^3\ {}^2D_{3/2}$-$^2D_{5/2}$. In a previous measurement at the Livermore SuperEBIT device [10], the wavelength of this line was determined to be about 3464 ± 2 Å. This measurement utilized a 1 m Acton normal incidence spectrometer with relatively low resolving power. The wavelength determined by our measurement agrees with our previous measurement within the uncertainty region, (we attribute this difference to the higher spectral resolution achieved in the present measurement), but differs from the NIST measurements [8] by almost 2 Å. Because this line is located at the edge of our measurement region, we investigated the reliability of our measurement of this line. One possible error could be that there was one calibration line (Ne II at 3459.32 Å) on the shorter wavelength side of this line, and misidentification of the calibration line could cause error on the wavelength determination. We did calibration fitting with and without the 3459.32 Å line, and found no significant difference in the wavelength calibration. Reassigning the Ne II line to another possible wavelengths, namely 3456.61 Å (Ne II) or 3460.524 Å (Ne I), would result in a break in the linearity of the spectral dispersion at this region. This does not seem to be convincing since the linearity in all other cases is quite consistent. However, we point out that this line may be affected by blends with lines from low charge states. This is a general problem for all

Table II. *Visible lines from highly charged Kr ions.*

E (beam) (eV)	Relative intensity	Wavelength (Å)	Ion charge state	I_p (eV) [(a)]	Transition
(500)[(c)]	30	3609.1 ± 0.5	$\leqslant$ Kr XVI	490.1	(b)
(970)[(c)]	10	3609.9 ± 0.5	$\leqslant$ Kr XXIII	935.4	(b)
(970)[(c)]	10	3600.0 ± 0.4	$\leqslant$ Kr XXIII	935.4	(b)
900	120	3466.6 ± 0.2	Kr XXII	885.5	$3s^2 3p^3\ {}^2D_{3/2}$-$^2D_{5/2}$ [8,10]
350	40	3586.1 ± 0.5	Kr V-Kr XI	<310	(b)
970	1000	3841.1 ± 0.2	Kr XXIII	935.4	$3s^2 3p^2$ ($^3P_1$-$^3P_2$) [8,11,23]
(3100)[(c)]	14	3739.1 ± 0.3	$\leqslant$ Kr XXIX	3068.6	(b)

(a) Ionization potential of the next lower-charge state ion to overcome in making the ions of interest [24].
(b) Atomic transition not available.
(c) The electron energy where the observation was made. The line could have been produced at smaller electron beam energies.

such measurements given the high density of lines from low charge states.

The third strongest line is at 3586.1 ± 0.5 Å. We could not narrow down the range of charge state of this line. This line did not exist in a spectrum taken in the inverted trap mode; it appeared clearly at an electron energy of 350 eV. The charge state of the ion that emits this line therefore is likely within the range of Kr^{4+}-Kr^{10+}.

Several other lines we found are quite weak, as shown in brackets in Table II. Because the lines are too weak for us to clearly determine their charge states (judging by their appearance on the spectra taken at different energies), we present the data where the observations were made, and without excluding the possibility that the lines might appear at smaller electron beam energies. Figure 3 shows one of the weak lines from a highly charged Kr ion, which was observed best at an electron energy of 3300 eV at a wavelength of 3739.1 ± 0.3 Å. Because of its threshold energy, we attribute the line to charge states less or equal than Kr^{18+}.

Other than the Si-like ion Kr line at 3841.1 Å and the P-like Kr ion line at 3466.6 Å, the atomic transitions for the rest of the lines are not yet known. One reason for this is that theory so far is unable to predict the fine structure intervals in many-electron heavy ions with sufficient accuracy. There are numerous tabulated predictions (of which we just list a few representative examples) on transitions in the $n = 2$ ground complex in Li- to F-like ions [25] as well as on the $n = 3$ ground complex in Al- to Cl-like ions [26–40], and on levels up to the $n = 3$ shell in Ne-like ions [41], as well as semi-empirically adjusted systematization of many forbidden transitions [23]. However, none of these provides suitable candidates to identify our lines with. The next group of levels to consider is the 3d level, some of which have a total angular momentum J that is at least two units higher than that of any level in the ground complex, so that low-rate M2 and similar high-multipole order transitions may be dominant decay branches of consequently long-lived levels. Some of these levels make prime candidates for our unassigned lines. However, predictions of these levels and their decay properties are both incomplete and suffer from large uncertainties of the calculated level energy differences – while the experiment suffers from the fact that at most one out of several decay branches of a given 3d level would fall into our range of observation, leaving only a fraction of the total level population to be observed via a given line.

Table III provides more detailed information on the measured line features. Fitted wavelengths and the errors (in brackets) are given in the first Column. It is noted that many line features appeared in the measured spectra; but only those which are relatively strong (relative intensity close to and above 10) are listed in the table. Most of the listed line features are from low charge state ions observed in the inverted-trap mode. The charge states of these ions are expected to be in the range from neutral to 3 or 4 times ionized atoms. Some spectral features appeared weakly in the inverted trap spectra, such that they could not be fitted properly. In order to determine the wavelength of these weaker lines, we fitted them using data acquired at higher electron beam energies (typically 350–1000 eV). Because there were weak indications of some of those lines existing under inverted-trap conditions, we could not determine the charge states of some of the lines, which we then labeled

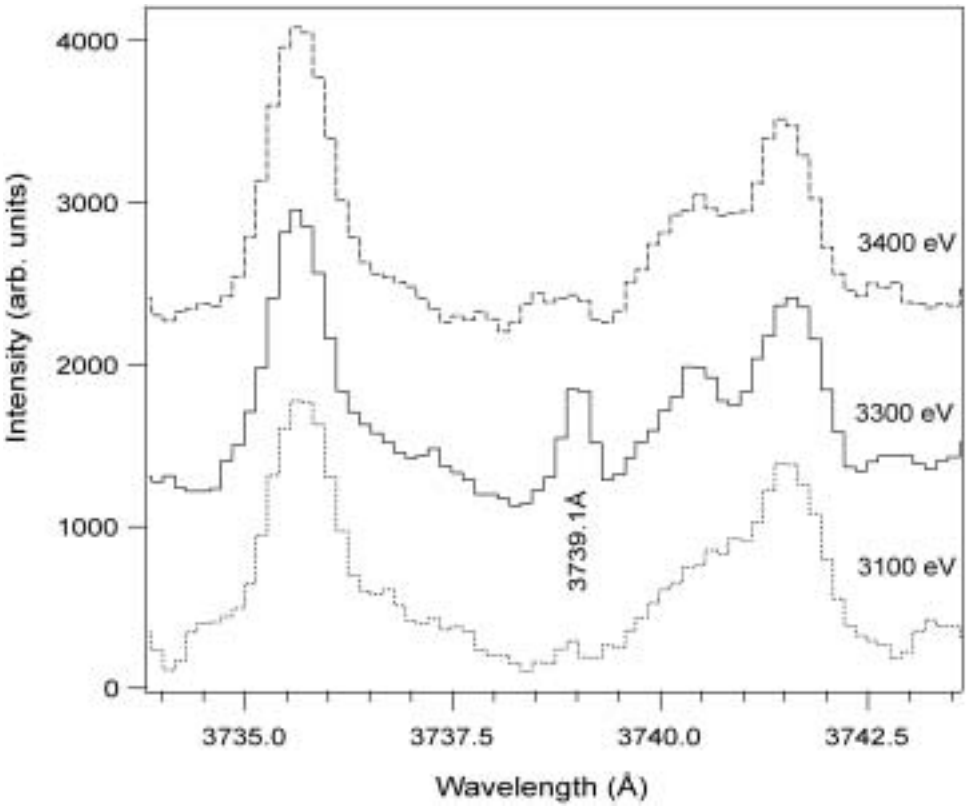

Fig. 3. Sections of Kr spectra at three electron beam energies, 3400 eV (top), 3300 eV (middle) and 3100 eV (bottom). A line that appears at a beam energy of 3300 eV is consequently attributed to Kr XXVIII.

Table III. *Summary of Kr lines measurements.*

Wavelength (Å)[a]	Relative intensity[a]	Trap condition[a]	Ion charge state[a]	Wavelength (Å)[b]	Ion charge state[b]	Ref.
3466.6(2)	120	900 eV	Kr XXII	3464.7 ± 0.6	Kr XXII	[8]
3467.3(2)	60	Indeterminate				
3469.9(2)	22	Inverted Trap	Kr I-Kr V			
3474.5(2)	16	Inverted Trap	Kr I-Kr V	3474.65	Kr III	[3]
3488.4(2)	50	Inverted Trap	Kr I-Kr V	3488.59	Kr III	
3492.5(5)	14	Inverted Trap	Kr I-Kr V			
3497.0(2)	16	Inverted Trap	Kr I-Kr V			
3498.2(3)	12	Inverted Trap	Kr I-Kr V			
3507.3(3)	82	Inverted Trap	Kr I-Kr V	3507.42	Kr III	[3]
3514.3(2)	12	Inverted Trap	Kr I-Kr V			
3534.8(3)	24	Indeterminate				
3535.5(2)	32	Inverted Trap	Kr I-Kr V			
3549.9(2)	18	Inverted Trap	Kr I-Kr V			
3554.8(2)	8	Inverted Trap	Kr I-Kr V			
3555.7(2)	18	Indeterminate				
3564.2(2)	50	Inverted Trap	Kr I-Kr V	3564.23	Kr III	[3]
3567.5(3)	10	Indeterminate				
3586.1(5)	40	350 eV	Kr V - Kr XI			
3589.4(4)	16	Inverted Trap	Kr I-Kr V			
3599.0(4)	14	Inverted Trap	Kr I-Kr V			
3600.0(4)	10	⩽970 eV	⩽Kr XXIII			
3607.9(4)	32	Inverted Trap	Kr I-Kr V	3607.88	Kr II	[4]
3609.1(5)	30	⩽500 eV	⩽Kr XVI			
3609.9(5)	10	⩽970 eV	⩽Kr XXIII			
3615.7(5)	8	Indeterminate				
3623.6(5)	10	Inverted Trap	Kr I-Kr V			
3631.9(4)	8	Inverted Trap	Kr I-Kr V	3631.889	Kr II	[5]
3637.7(4)	12	Inverted Trap	Kr I-Kr V			
3641.3(5)	20	Inverted Trap	Kr I-Kr V	3641.34	Kr III	[3]
3648.5(4)	16	Inverted Trap	Kr I-Kr V			
3660.3(4)	11	Inverted Trap	Kr I-Kr V			
3665.3(5)	45	Indeterminate				
3667.6(4)	20	Inverted Trap	Kr I-Kr V			
3680.4(5)	10	Inverted Trap	Kr I-Kr V			
3686.1(2)	32	Indeterminate				
3690.7(2)	24	Inverted Trap	Kr I-Kr V	3690.65	Kr III	[21]
3696.7(3)	12	Indeterminate				
3712.9(3)	10	Indeterminate				
3718.4(2)	46	Inverted Trap	Kr I-Kr V	3718.595	Kr II	[5]
3721.4(2)	38	Inverted Trap	Kr I-Kr V	3721.35	Kr II	[5]
3726.4(3)	14	Indeterminate				
3732.8(2)	25	Inverted Trap	Kr I-Kr V			
3735.8(2)	31	Inverted Trap	Kr I-Kr V			
3739.1(3)	14	⩽3100 eV	⩽Kr XXIX			
3740.5(3)	13	Inverted Trap	Kr I-Kr V			
3741.7(2)	20	Inverted Trap	Kr I-Kr V	3741.638	Kr II	[5]
3744.8(2)	72	Inverted Trap	Kr I-Kr V	3744.8	Kr II	[4]
3747.7(4)	8	Indeterminate				
3749.5(3)	14	Indeterminate				
3754.3(2)	54	Inverted Trap	Kr I-Kr V	3754.245	Kr II	[5]
3759.2(2)	12	Inverted Trap	Kr I-Kr V			
3765.6(3)	10	Inverted Trap	Kr I-Kr V			
3771.2(2)	20	Inverted Trap	Kr I-Kr V			
3773.4(3)	11	Inverted Trap	Kr I-Kr V			
3776.5(3)	8	Inverted Trap	Kr I-Kr V			
3777.9(2)	17	Inverted Trap	Kr I-Kr V	3778.089	Kr II	[5]
3783.0(2)	8	Inverted Trap	Kr I-Kr V	3783.095	Kr II	[5]
3785.6(2)	47	Inverted Trap	Kr I-Kr V			
3788.0(2)	14	Inverted Trap	Kr I-Kr V			
3792.6(2)	31	Inverted Trap	Kr I-Kr V			
3795.6(3)	10	Inverted Trap	Kr I-Kr V			
3804.8(3)	8	Indeterminate				
3806.0(3)	12	Inverted Trap	Kr I-Kr V			
3817.4(2)	10	Inverted Trap	Kr I-Kr V			
3819.9(3)	10	Inverted Trap	Kr I-Kr V			
3822.2(3)	12	Inverted Trap	Kr I-Kr V			
3832.0(2)	80	Inverted Trap	Kr I-Kr V			
3835.0(2)	50	Inverted Trap	Kr I-Kr V			
3836.8(2)	68	Inverted Trap	Kr I-Kr V			

Table III. *Continued.*

Wavelength (Å)[a]	Relative intensity[a]	Trap condition[a]	Ion charge state[a]	Wavelength (Å)[b]	Ion charge state[b]	Ref.
3841.1(2)	1000	970 eV	Kr XXIII	3832; 3840.9 ± 0.3; 3841.4 ± 0.2	Kr XXIII	[21]; [7]; [11]
3844.4(2)	83	Inverted Trap	Kr I-Kr V			
3857.1(2)	15	Inverted Trap	Kr I-Kr V			
3858.5(2)	14	Inverted Trap	Kr I-Kr V			
3860.3(3)	14	Inverted Trap	Kr I-Kr V	3860.58	Kr IV	[19]
3864.7(3)	16	Inverted Trap	Kr I-Kr V			
3868.7(2)	20	Inverted Trap	Kr I-Kr V	3868.7	Kr III	[3]
3872.7(2)	24	Inverted Trap	Kr I-Kr V			
3875.4(2)	60	Inverted Trap	Kr I-Kr V	3875.44	Kr II	[4]

[a]Present measurements.
[b]Data from references listed in the last column.

as indeterminate. Few lines appeared only at higher electron beam energies, and the probable ion states of these lines (Column four) are given in the table.

The previously measured lines are given in the last three columns as references. We note that the plasma conditions in our work are different from those in the earlier observations of transitions in neutral and low-charge state ions, which generally were characterized by a higher electron density than that of the present measurements. We list the relative intensity of the observed lines in Table III in order to enable comparisons with optical models that may be developed in the future.

Acknowledgements

This work was performed under the auspices of the U.S. Department of Energy by the University of California Lawrence Livermore National Laboratory under contract No. W-7405-Eng-48, and supported by the Chemical Sciences, Geosciences and Biosciences Division of the Office of Basic Energy Science, Office of Science. We gratefully acknowledge extensive discussions with E. Träbert who also made helpful suggestion for this presentation. We also thank the referee for very constructive comments.

References

1. Samm, U. *et al.*, in "Plasma Physics and Controlled Nuclear Fusion Research 1992", **1**, IAEA, Vienna 309 (1993).
2. Post, D. *et al.*, Phys. Plasmas **4**, 2631 (1997).
3. Humphreys, C. J., Phys. Rev. **47**, 712 (1935).
4. de Bruin, T. L., Humphreys, C. J. and Meggers, Wm. F., Bur. Standards, J. Research **11**, 409 (1933).
5. Humphreys, C. J. and Paul, E. jr., J. Opt. Soc. Am. **60**, 200 (1970).
6. Rao, A. B. and Kirshnamurty, S. G., Proc. Phys. Soc (London) **51**, 772 (1939).
7. Roberts, J. R., Pittman, T. L., Sugar, J., Kaufman, V. and Rowan, W. L., Phys. Rev. A **35**, 2591 (1987).
8. Serpa, F. G., Bell, E. W., Meyer, E. S., Gillaspy, J. D. and Roberts, J. R., Phys. Rev. A **55,** 1832 (1997).
9. Crespo López-Urrutia, J. R., Beiersdorfer, P., Widmann, K. and Decaux, V., Physica Scripta T **80**, 448 (1999).
10. Träbert, E., Beiersdorfer, P., Utter, S. B. and Crespo López-Urrutia, J. R., Physica Scripta **58**, 599 (1998).
11. Träbert, E., Utter, S. B. and Beiersdorfer, P., Phys. Lett. A **272**, 86 (2000).
12. Levine, M. A., Marrs, R. E., Henderson, J. R., Knapp, D. A. and Schneider, M. B., Physica Scripta T **22**, 157 (1988).
13. Beiersdorfer, P. *et al.*, in "Atomic Data Needs for X-ray Astronomy", (Eds. M. A. Bautista, T. R. Kallman and A. K. Pradhan), (NASA Goddard Space Flight Center, 2000), available on-line at http://heasarc.gsfc.nasa.gov/docs/heasarc/atomic/
14. Utter, S. B., Beiersdorfer, P. and Brown, G. V., Phys. Rev. A **61**, 030503 (2000).
15. Utter, S. B., Ph.D. thesis, Auburn University; available as Lawrence Livermore National Laboratory reprints No. UCRL-LR-139295, (2000).
16. Nguyen, H. T. *et al.*, Opt. Lett. **22**, 142 (1997).
17. Beiersdorfer, P., Decaux, V., Elliott, S. R. and Widmann, K., Rev. Sci. Instrum. **66**, 303 (1995).
18. Beiersdorfer, P., Osterheld, A. L., Decaux, V. and Widmann, K., Phy. Rev. Lett. **77**, 5353 (1996).
19. Porto, J. V., Kink, I. and Gillaspy, J. D., Rev. Sci. Instrum. **71**, 3050 (2000).
20. Chen, H. *et al.*, Physica Scripta **T92**, 284 (2001).
21. "CRC handbook of chemistry and physics: a ready-reference book of chemical and physical data" editor-in-chief, David R. Lide. 68rd ed. (Publisher Boca Raton, FL: CRC Press 1987–1988) pp E-201–E-327.
22. "NIST Atomic Spectra Database", Web based Version 2.0, http://physics.nist.gov (2000).
23. Kaufman, V. and Sugar, J., J. Phys. Chem. Ref. Data **15**, No. 1 (1986).
24. Scofield, J. H., private communication.
25. Cheng, K.-T., Kim, Y.-K. and Descaux, J. P., At. Data Nucl. Data Tables **24**, 111 (1979).
26. Huang, K.-N., Kim, Y.-K., Cheng, K. -T. and Desclaux, J. P., At. Data Nucl. Data Tables **28**, 355 (1983).
27. Huang, K.-N., At. Data Nucl. Data Tables **30**, 313 (1984).
28. Huang, K.-N., At. Data Nucl. Data Tables **32**, 503 (1985).
29. Huang, K.-N., At. Data Nucl. Data Tables **34**, 1 (1986).
30. Mendoza, C. and Zeippen, C. J., Mon. Not. R. Astron. Soc. **198**, 127 (1982).
31. Mendoza, C. and Zeippen, C. J., Mon. Not. R. Astron. Soc. **199**, 1025 (1982).
32. Mendoza, C. and Zeippen, C. J., Mon. Not. R. Astron. Soc. **202**, 981 (1983).
33. Bhatia, A. K. and Doschek, G. A., At. Data Nucl. Data Tables **53**, 23 (1993).
34. Bhatia, A. K. and Kastner, S. O., J. Quant. Spectrosc. Radiat. Transfer **49**, 609 (1993).
35. Bhatia, A. K. and Doschek, G. A., At. Data Nucl. Data Tables **60**, 973 (1995).
36. Bhatia, A. K. and Doschek, G. A., At. Data Nucl. Data Tables **64**, 183 (1996).
37. Biémont, E. and Hansen, J. E., Physica Scripta **34**, 116 (1986).
38. Biémont, E. and Hansen, J. E., Physica Scripta **31**, 509 (1986).
39. Biémont, E. and Bromage, G. E., Mon. Not. R. Astron. Soc. **205**, 1085 (1983).
40. Kohstall, C., Fritzsche, S., Fricke, B. and Sepp, W. -D., At. Data Nucl. Data Tables **70**, 63 (1998).
41. Hibbert, A., Le Dourneuf, M. and Mohan, M., At. Data Nucl. Data Tables **53**, 23 (1993).

